A simple model of the scanning near-field optical microscopy probe tip for electric field enhancement

YINGJIE WANG, WEI CAI, MU YANG, ZHENGLIANG LIU, GUANGYI SHANG[*]

Department of Applied Physics, Beihang University, Beijing 100191, China

[*]Correspondence author: gyshang@buaa.edu.cn

In this paper, we present a simple near-field probe model that is composed of an elongated ellipsoid and a finite metal truncated cone. The elongated ellipsoid has been shown to act as a protrusion or separate particle near a truncated cone apex with strong near-field enhancement under laser excitation. By controllably varying the length of the ellipsoid protrusion from the truncated cone, the truncated cone-ellipsoid probes can be adapted to the suitability of near-field probes. The effects of substrate material and excitation wavelength on the near field enhancement for different tip apexes are also discussed. In addition, we compared the properties of the truncated cone-ellipsoid probe with the widely used hemisphere conical tip by launching surface plasmon polaritons on plasmonic waveguides to prove the suitability of the truncated cone-ellipsoid probes as high performance near-field probes. The present simple model would provide a theoretical basis for the actual construction of probes.

Keywords: near-field tip, electromagnetic field enhancement, finite-different time-domain (FDTD).

1. Introduction

Benefits from the use of a sharp tip, scanning near-field optical microscopy (SNOM) and tip-enhanced Roman spectroscopy (TERS) methods have the capability of direct probing optical properties of inorganic, organic, and biological materials on a nano-meter-scale [1–4]. Theoretical and experimental studies have shown that the high resolution is the result of a strongly localized electric field [5–7] and great field enhancement [8, 9] produced near the tip apex. One of important issues is that we should choose the optimal conditions to achieve as maximal near-field enhancement as possible for detection with the high resolution.

Over the last two decades, a variety of near-field tips have been proposed in literature, which could be mainly categorized into two types: aperture and apertureless [10–12]. The aperture-based tips can achieve the resolution of optical images better than 50 nm, breaking the diffraction limit on spatial resolution [13, 14]. However, the light through-put decreases markedly as the aperture diameter decreases and a large aperture leads

to a relatively poor resolution [15, 16]. Equally challenging is the fabrication of tips with sufficiently small apertures to resolve small topographic features [17–19]. The alternative method is an apertureless-based probe, which uses a sharp tip as either a local field scatter or a locally enhanced optical source. These tips show strong field confinement and enhancement upon external far-field illumination due to the lighting-rod effect and the excitation of localized surface plasmons. The high spatial resolution of 3 nm, limited only by the sharpness of the tip apex diameter [20], has been demonstrated. However, since the far-field illumination by a focused laser beam generates a large background scattering signal, highly localized light at the tip apex is very desirable, which could significantly suppress interferences with a background from far-field illumination [21–23].

A proper tip should possess nano-scale resolution, efficient far-field to near-field coupling, strong local field enhancement, and perhaps most importantly, reproducibility and robustness [24]. In recent years, a variety of apertureless tips aimed at improving one or more of these desired tip properties have been proposed, including an etched metal tip [21], a metal coated silicon cantilever [25], a nanoparticle attached to the apex of a tapered optical fiber or a cantilever [5, 26]. In particular, plasmonic tips with arrays of subwavelength holes, slits and other plasmonic planar geometries on the side or apex of the tip [8, 27] have been developed, which are able to achieve better enhancement and confinement. In the aspect of numerical simulation, most literature established the calculation model of the apertureless tips and did optical property analysis for a probe tip of different structure parameters with a software. These models include a semi-infinite solid of a conical or pyramidal shape [28], a finite cylinder [29], truncated cone [30], and circular cylinder with tapered ends [31].

In the reported literatures, Martin *et al.* [32] put forward a point of view that the retardation effects can drastically reduce the electric field enhancement, and changing the tip area illuminated by a laser beam results in unstable enhancement of the local electric field near the apex. To overcome these problems, one of possible solutions is to create a small discontinuity at the tip end, which is a protrusion or separate particle made of a different material. In fact, several theories have proposed a metal particle probe, which is composed of a cantilever or optical fiber with metal particle [5, 26, 33]. According to their proposals, we present a simple near-field probe model that is composed of an elongated ellipsoid and a finite metal truncated cone. The elongated ellipsoid can be used as a protrusion or separate particle in terms of the feature of structural organization. In the studying, we have made great efforts to give an optimization design in order to achieve the best structural layout. The effects of substrate material and excitation wavelength on the near-field enhancement for different tip apex are also discussed. Finally, we compared the properties of the truncated cone-ellipsoid probe with the widely used hemisphere conical tip by launching surface plasmon polaritons (SPP) on plasmonic waveguides to prove the suitability of the truncated cone-ellipsoid probes as high performance near-field probes. The establishment of the model provides a theoretical basis for the actual construction of the probe.

2. Simulation method and model

To study the effect of the tip shape on the electromagnetic field enhancement and optimize the probe tip design, various theoretical methods, such as the finite-difference time-domain (FDTD), have been developed [34]. Here, the three-dimensional finite-difference time-domain (3D-FDTD) method was used. In our simulation, the commercially available FDTD software (Lumerical Solutions, Inc., Vancouver, Canada) has been used [7]. Figure 1 shows the geometry of the model for our computer simulation. The probe is made up of a finite gold truncated cone and a gold elongated ellipsoid. The length of the truncated cone is $L = 800$ nm with diameters of the two ends of $D = 200$ nm and $d = 20$ nm, respectively. The length of the minor and major axis of ellipsoid are $d = 20$ nm and j. The length of the ellipsoid protrude from the truncated cone is δ, so the total length of the probe is $\pounds = L + \delta$. The probe is located near a flat surface of a substrate, and the distance between the probe and the substrate surface is $g = 8$ nm. The frequency power monitors record the electric fields which are located under the tip and the distance from the tip apex is h. In order to ensure the accuracy of the FDTD simulation results, some convergence tests were conducted to reduce the numerical error to an acceptable level. Most of error sources that lead to typically small effects can be ignored completely when the default settings were used. However, the
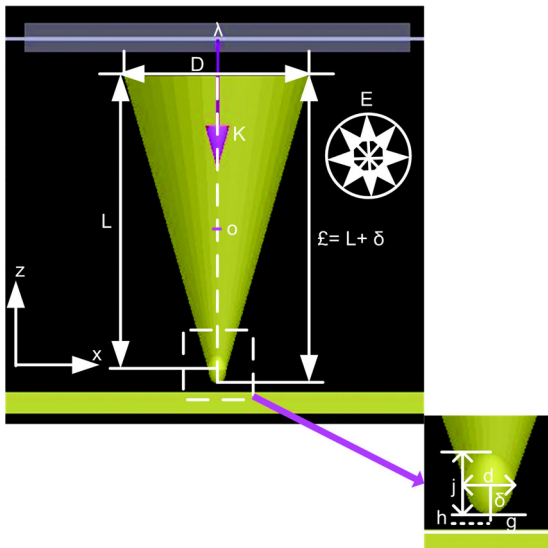
Fig. 1. Geometry of the composed apertureless tip model: the tip is made of a finite gold truncated cone and a gold elongated ellipsoid particle with a minor axis d and major axis j. The length of the truncated cone is $L = 800$ nm with diameters of the two ends of $D = 200$ nm and $d = 20$ nm, respectively. The ellipsoid exposed to the truncated cone is δ. So the total length of the probe tip is $\pounds = L + \delta$. The distance g between the tip apex and the substrate surface is 8 nm. The frequency power monitors record the electric fields which are located under the tip and the distance from the tip apex is h. The incident light is a Gaussian source with a radial polarization.

effects of perfectly matched layer (PML) reflectivity and grid size are important. Taking into account enough computational resources and the limits of our computer, the input parameters for the simulation were set as follows: the simulation volume was $1000 \times 1000 \times 1200$ nm discretized with an auto non-uniform mesh step surrounded by 64 layers of PML boundary conditions at all boundaries. PML reflectivity was set at 1×10^{-5}. A non-uniform mesh was automatically generated based on the mesh accuracy slider bar and the material properties. In this case, the mesh accuracy parameter was set at 4, and the step-size depends on $(1/18 \times \lambda/n)$, where λ is the light wavelength and n is the index of the current material. Overriding meshes were set to ensure finer grid spacing at points of interest. A grid with spacing of 0.5 nm was created around the gap between the tip and the substrate, since it is known that the nano-gap region is often characterized by a rapid increase in electric field intensity. Simulation time step was $\nabla t = 9.53 \times 10^{-18}$ s. A Gaussian beam light source was used. According to [35–38], the radial polarization of the incident light promotes the stronger confinement of the electric field than a linearly input polarization. So the radially polarized light with the wavelength of 633 nm was utilized for the corresponding calculations. The polarization vectors were oriented radially in the transverse plane with respect to the propagation direction (z axis). All the calculated and reported intensities are normalized with respect to the intensity of the incident light.

3. Results and discussion

Figure 2 displays five structures of such composed tip and corresponding simulation results of the electric field distribution, respectively. As can be seen in Fig. 2**a**, the elec-
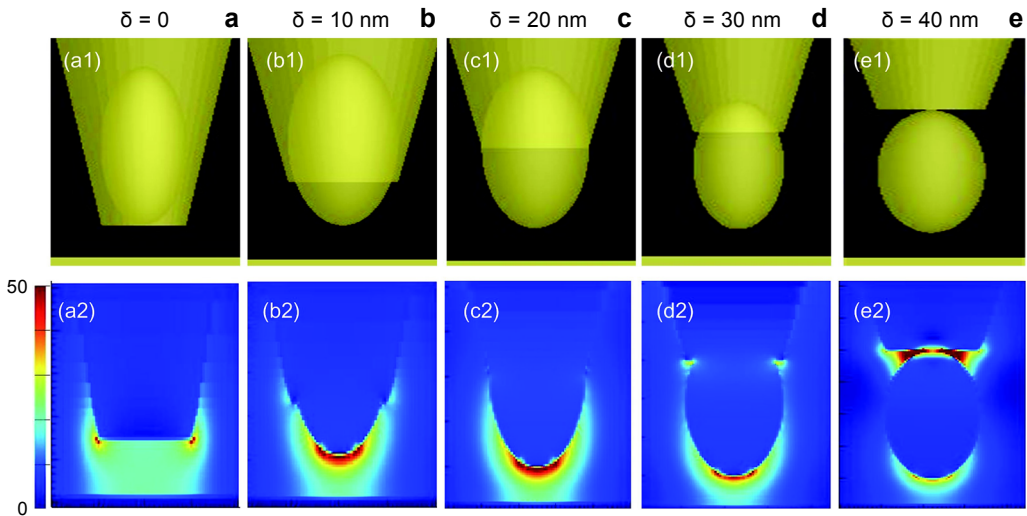
Fig. 2. The structures and the electric field distributions of the tip model in the *x-z* section for $\delta = 0$ (**a**), $\delta = 10$ nm (**b**), $\delta = 20$ nm (**c**), $\delta = 30$ nm (**d**), and $\delta = 40$ nm (**e**) of the ellipsoid protrude from the truncated cone.
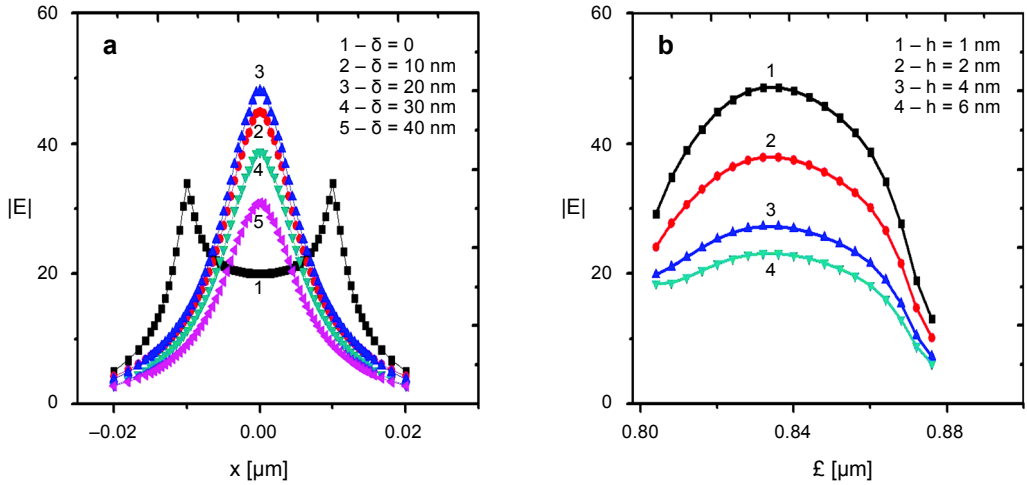
Fig. 3. The variations in electric field $|E|$ as a function of the x for the different values δ, and the frequency power monitors position is $h = 4$ nm (**a**). Calculated variation in the electric field $|E|$ as a function of probe tip model length $£$ for different position h (**b**). The length of minor and major axis of ellipsoid are $d = 20$ nm and $j = 40$ nm, respectively, and the wavelength of incident light is 633 nm.

tric field is enhanced at the side points of the top edge of the truncated cone when the length of an ellipsoid protrude from the truncated cone is $\delta = 0$. If the ellipsoid protrudes from the truncated cone, as shown in Figs. 2**b**–2**d**, the field distributions change with the protrusion length δ and the field enhancement takes place only at the probe tip. When the ellipsoid is jointed in the truncated cone, as shown in Fig. 2**e**, which is like a metal particle probe, the electric field is enhanced not only at the probe tip but also in the gap between the top of the truncated cone and the ellipsoid. Further, we calculated the variations in electric field $|E|$ as a function of the x for different values δ, and the frequency power monitors record the electric fields which are located under the tip and the distance from the tip apex is $h = 4$ nm, as shown in Fig. 3**a**. It is easy to see that the center part underneath the tip has higher intensity and the maximum intensity can be obtained in the case of x being 0 and δ being 20 nm, which is the half-length of the ellipsoid major axis. These simulation results, consistent [18], are used to prove that the variation of the local field intensity depends on how smooth is the joint surface between the ellipsoid and the truncated cone. There are no abrupt steps or small gaps between the cone and the ellipsoid when $\delta = 20$ nm, so the electric field mainly distributes on the apex rather than anywhere else. Figure 3**b** gives the variation in the electric field $|E|$ as a function of probe tip model length $£$ for different position h. We can also see that the maximum electric field intensity can be obtained for $\delta = 20$ nm. In addition, the local field enhancement is decreased when h increases. This is because the electric field collects near the tip apex, and the electric field will decrease with increasing distance from the tip apex.

From the results of Fig. 2, we known that the maximum electric field intensity can be obtained when the ellipsoid just protrudes from the truncated cone and the extension
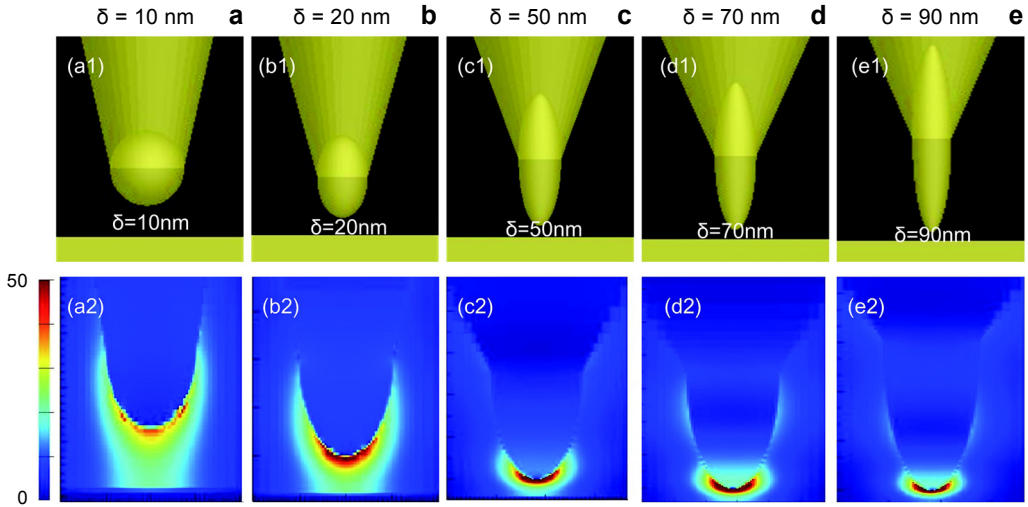
Fig. 4. The structures and the electric field distributions of the probe tip model. The ellipsoid protrude from the truncated cone and the extension length equal to the half-ellipsoid major axis. Most geometrical parameters are held constant, and the extension lengths are $\delta = 10$ nm (**a**), $\delta = 20$ nm (**b**), $\delta = 50$ nm (**c**), $\delta = 70$ nm (**d**), and $\delta = 90$ nm (**e**).

length equal to the half-ellipsoid major axis. Here, we consider the effect of one geometrical parameter of the ellipsoid tip, namely, the length of the half-ellipsoid major axis δ, on the electric field enhancement. The results are given in Figs. 4**a**–4**e**, the ellipsoid major axis becomes longer (*i.e.*, $\delta = 10, 20, 50, 70,$ and 90 nm, respectively).
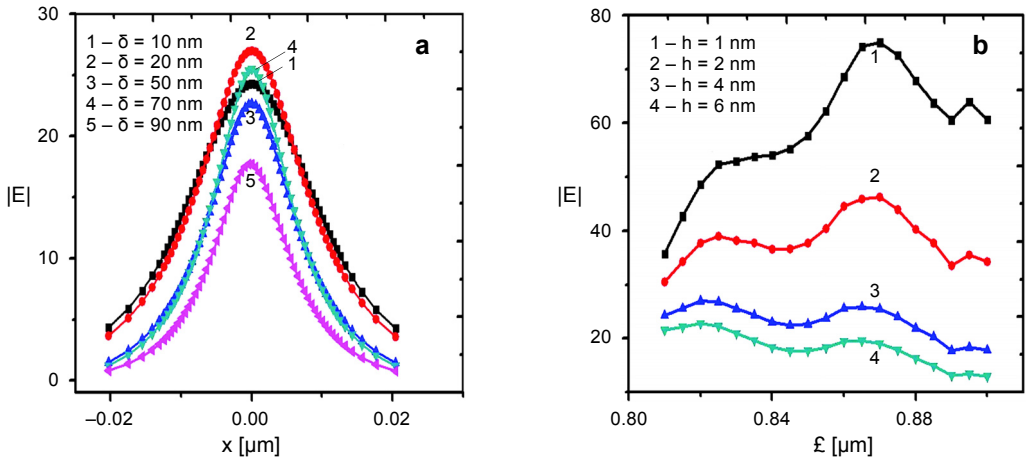
Fig. 5. The variations in electric field $|E|$ as a function of the x for the different values δ; the frequency power monitors record the electric fields are located under the tip and the distance from the tip apex is $h = 4$ nm (**a**). Calculated variation in the electric field $|E|$ as a function of probe tip model length $\pounds$ for different position h (**b**). The wavelength of incident light is 633 nm.

It is easy to find that the field enhancement accumulates mainly at the sharp tip apex and depends essentially on the tip length £. To understand this behavior in more detail, further simulations have been performed. Figure 5**a** depicted the variations in electric field |E| as a function of the x for the different values δ, and the frequency power monitors position is h = 4 nm. The figure clearly indicates that the field enhancement underneath the tip apex is not linearly increasing with the increase in the extension length δ. The maximum field enhancement could be obtained when the extension length δ is 20 nm, which is larger than that of the extension length δ = 10 nm. And the probe has been described as the rounded cone in other published simulations if the extension length δ is 10 nm [26, 39]. Figure 5**b** shows the variation in the electric field |E| as a function of probe tip model length £ for different position h. It is clear that two prominent peaks appear in local field spectra of the tip in all different observation planes. That means the electric field enhancement is larger when the length of the extension δ is 20 and 70 nm, respectively. Beyond that, the electric field enhancement will decrease with the increase of h. Most likely, the combined effects of the multipole effect of the nanoantenna and the lighting rod influence the results.

Furthermore, we calculate the electric field enhancement *versus* the extension length δ for different wavelength as shown in Fig. 6**a**. In the calculation, the Au substrate is used and the distance between the tip and the substrate is set to be 8 nm. Taking 532, 633, 830, and 1000 nm into consideration, the calculated results present that the maximum field enhancement appears at different values of the extension length δ. If the excitation wavelength is 633 nm, the highest field enhancement is achieved in the case of δ being 20 and 70 nm. Based on the present understanding for plasmon resonance of small particles, the new high-frequency modes of multipolar order emerge
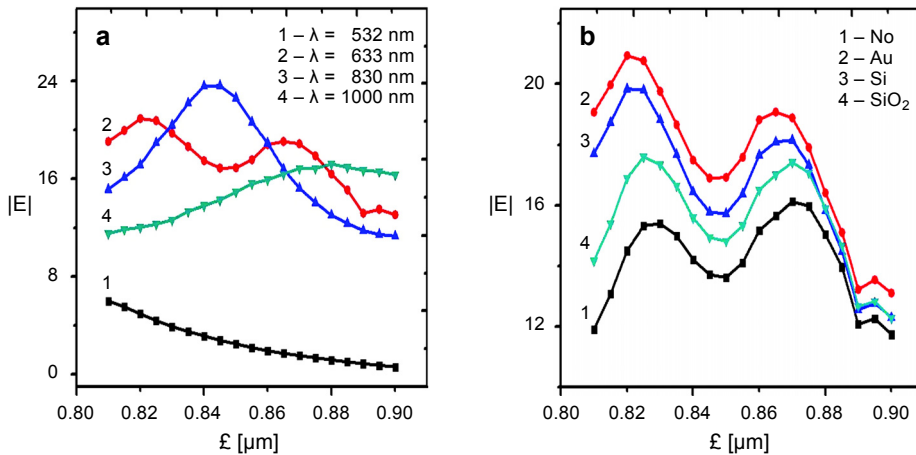
Fig. 6. The electric field enhancement |E| *versus* the probe length £ for different wavelength (the gold substrate) (**a**) and different substrate (λ = 633 nm) (**b**). Most geometrical parameters are held constant; the ellipsoid protrudes from the truncated cone and the extension length is equal to the half-ellipsoid major axis, and δ = 20 nm; the frequency power monitors position is h = 4 nm.

for extended objects [39]. For the probe length at 820 nm, there might be a resonance peak at 633 nm for the dipolar mode; for the probe length at 870 nm, there might be another higher-order resonance mode, since as the length of nanoantenna increases, the frequency of mode red shifts, which insures the higher-order modes to enter the 633 nm region. The lightning rod effect, resulting from the increasing confinement of the surface charge density at the sharp tip apex, is a non-resonant effect, which depends mainly on the radius of curvature of the tip [4]. Earlier calculations for long tips show that the field enhancement decreases moderately with increasing tip length and radius [6, 11, 21]. In our simulations, the length of tip extension is increasing, but the radius of the tip is decreasing with the increase of δ. Therefore, the variation of the field enhancement value is the result of the multipole effect of the nanoantenna and the lighting rod effect.

From Figure 6**a**, we can also see that the effect of the excitation wavelength on the field enhancement of different tip apexes is not trivial. The optimal tip length $\pounds$ is distinct for different excitation wavelength. If the excitation wavelength is 532 nm, the highest field enhancement is achieved in the case of δ being 10 nm, which is a hemisphere shape. Therefore, the ellipsoid shape of the tip apex lost its advantage. The highest ratio of field enhancement between the extension length and the hemisphere tip apex is achieved for the excitation wavelength of 830 nm and $|E|_{\delta = 40 \text{ nm}}/|E|_{\delta = 10 \text{ nm}} = 1.6$. This phenomenon can be explained as follows. On the one hand, the enhancement essentially depends on the plasmonic resonance of small particles. The resonant modes experience a red shift and new high-frequency modes of multipolar order emerge for extended objects. On the other hand, the near field is thus practically determined by the surface charge density near the apex. Increasing the length $\pounds$ of the tip results in reducing the curvature and enlarging the surface area near the tip. The sharper the curvature is, the higher the surface charge distribution is. The relatively large surface area will lead to a decrease in the surface charge density and hence to a decrease in the electric field.

In order to study the influence of substrate materials on the field enhancement, Au, Si and SiO_2 are chosen as the substrate materials. The distance between the tip apex and the substrate is fixed at 8 nm. The radially polarized Gaussian source with a wavelength of 633 nm is used as the incident light. The intensity curves for the different tip length $\pounds$ and different substrate materials are shown in Fig. 6**b**, where the dependence of the enhancement on the tip length $\pounds$ has the same form for all simulation results, but the magnitudes of the intensity are different. The Au substrate provides the highest field enhancement, while the dielectric substrates (Si, SiO_2) are in the middle between the Au substrate and no substrate. These results imply that the coupling degree between the tip and the substrate effects the enhancement. The metallic tip-substrate structure is able to provide strong surface plasmonic resonances in the visible range.

In order to demonstrate the advantage of the truncated cone-ellipsoid tip, the launching of SPP on plasmonic waveguides using the truncated cone-ellipsoid tip was studied
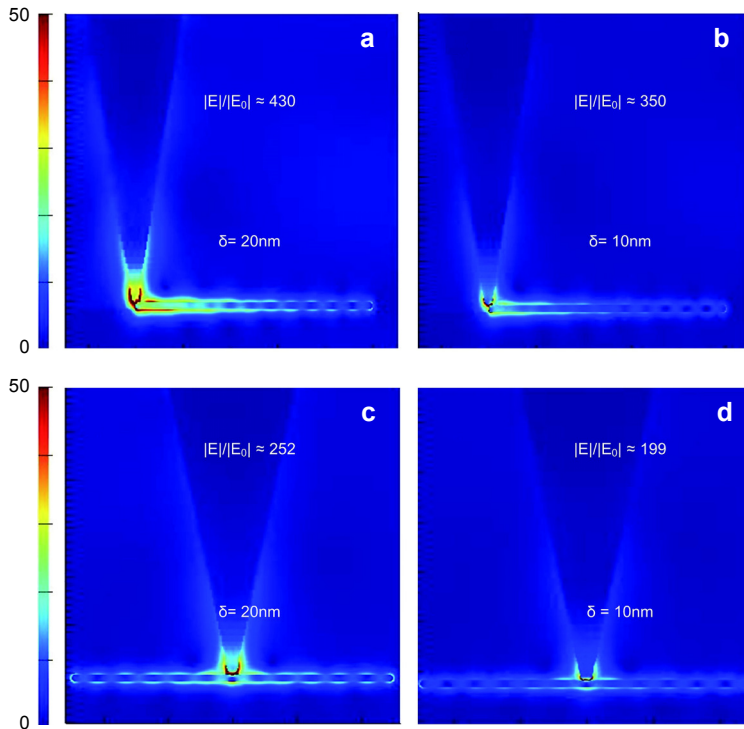
Fig. 7. Simulations of the electric field distribution for the tip at the left end (**a**, **b**) and the midsection (**c**, **d**) of the Ag nanowire, put on the SiO$_2$ substrate. The diameter and the length of the Ag nanowire are 10 and 1000 nm, respectively.

and compared with the widely used conical tip [28, 40]. The simulation results of the field distribution are given in Fig. 7, in which the length of the truncated cone-ellipsoid tip extension δ is 20 nm and that of the conical tip is 10 nm. An gold nanowire is placed on the SiO$_2$ substrate and the incident light wavelength is 633 nm. As shown in Fig. 7, an increase of the field enhancement at the junction between the tip and the nanowire takes place. The enhancement factors of 430 and 252 can be obtained with the truncated cone-ellipsoid tip while illuminating the end and the middle of the nanowire, respectively, which are higher than respective 350 and 199 with the conical tip at the same positions. The results imply that higher efficiency for launching SPP on the nanowire can be obtained by using the ellipsoid tip under the same conditions. The reason of the enhancement factors, while illuminating the end, are larger than those when illuminating the middle of the nanowire, could be explained as follows. Under normal circumstances, in order to couple light into SPP modes in a nanowire, momentum mismatch between the photons and the plasmons must be compensated. When the light through the tip apex directly illuminates one end of the nanowire (see Figs. 7**a** and 7**b**) or the middle of the nanowire (see Figs. 7**c** and 7**d**), efficient subwavelength-scale near the

field coupling emerges between the tip and the nanowire. The end-face scattering of the tip apex provides an additional wave vector and causes the mismatch of the momentum.

4. Conclusion

We have presented a numerical model of an apertureless probe for the SNOM and TERS methods based on the FDTD method. The probe consists of an elongated ellipsoid positioned at the top of a finite gold truncated cone. The elongated ellipsoid has been shown to act as a protrusion or separate particle near a truncated cone apex with strong near-field enhancement under laser excitation. A well-defined and adjustable near-field probe model is determined by the shape and size of the elongated ellipsoid. This probe concept combines the advantages of a very sharp tip for high spatial resolution, and the multipole effects of the optical antennas. Near-field enhancements from launching SPP on plasmonic waveguides were shown to prove the suitability of the truncated cone-ellipsoid probes as high performance near-field probes. The present simple model would provide an alternative way for fabrication of a tip with a high performance for the SNOM and TERS methods.

References

[1] Kodama T., Umezawa T., Watanabe S., Ohtani H., *Development of apertureless near-field scanning optical microscope tips for tip-enhanced Raman spectroscopy*, Journal of Microscopy **229**(2), 2008, pp. 240–246.

[2] Xudong Cui, Erni D., Weihua Zhang, Zenobi R., *Highly efficient nano-tips with metal–dielectric coatings for tip-enhanced spectroscopy applications*, Chemical Physics Letters **453**(4–6), 2008, pp. 262–265.

[3] Demming A.L., Festy F., Richards D., *Plasmon resonances on metal tips: understanding tip-enhanced Raman scattering*, The Journal of Chemical Physics **122**(18), 2005, article ID 184716.

[4] Zhilin Yang, Aizpurua J., Hongxing Xu, *Electromagnetic field enhancement in TERS configurations*, Journal of Raman Spectroscopy **40**(10), 2009, pp. 1343–1348.

[5] Tanirah O., Kern D.P., Fleischer M., *Fabrication of a plasmonic nanocone on top of an AFM cantilever*, Microelectronic Engineering **141**, 2015, pp. 215–218.

[6] Behr N., Raschke M.B., *Optical antenna properties of scanning probe tips: plasmonic light scattering, tip–sample coupling, and near-field enhancement*, The Journal of Physical Chemistry C **112**(10), 2008, pp. 3766–3773.

[7] Liu J.C., Liu D.M., Shao T.M., *FDTD simulation on laser-induced enhancement of electric field in the near-field apertureless probe system*, Laser Physics Letters **9**(7), 2012, pp. 511–518.

[8] Youngkyu Lee, Xiaojing Zhang, *Designs of apertureless probe with nano-slits for near-field light localization and concentration*, Optics Communications **285**(16), 2012, pp. 3373–3377.

[9] Novotny L., Pohl D.W., Hecht B., *Scanning near-field optical probe with ultrasmall spot size*, Optics Letters **20**(9), 1995, pp. 970–972.

[10] LINDQUIST N.C., JOSE J., CHERUKULAPPURATH S., XIAOSHU CHEN, JOHNSON T.W., SANG-HYUN OH, *Tip-based plasmonics: squeezing light with metallic nanoprobes*, Laser and Photonics Reviews **7**(4), 2013, pp. 453–477.

[11] HUBER C., TRÜGLER A., HOHENESTER U., PRIOR Y., KAUTEK W., *Optical near-field excitation at commercial scanning probe microscopy tips: a theoretical and experimental investigation*, Physical Chemistry Chemical Physics **16**(6), 2014, pp. 2289–2296.

[12] WESSEL J., *Surface-enhanced optical microscopy*, Journal of the Optical Society of America B **2**(9), 1985, pp. 1538–1541.

[13] POHL D.W., DENK W., LANZ M., *Optical stethoscopy: image recording with resolution λ/20*, Applied Physics Letters **44**(7), 1984, pp. 651–653.

[14] DÜRIG U., POHL D.W., ROHNER F., *Near-field optical-scanning microscopy*, Journal of Applied Physics **59**(10), 1986, pp. 3318–3327.

[15] BABADJANYAN A.J., MARGARYAN N.L., NERKARARYAN KH.V., *Superfocusing of surface polaritons in the conical structure*, Journal of Applied Physics **87**(8), 2000, pp. 3785–3788.

[16] JANUNTS N.A., BAGHDASARYAN K.S., NERKARARYAN KH.V., HECHT B., *Excitation and superfocusing of surface plasmon polaritons on a silver-coated optical fiber tip*, Optics Communications **253**(1–3), 2005, pp. 118–124.

[17] HAROOTUNIAN A., BETZIG E., ISAACSON M., LEWIS A., *Super-resolution fluorescence near-field scanning optical microscopy*, Applied Physics Letters **49**(11), 1986, pp. 674–676.

[18] BETZIG E., ISAACSON M., LEWIS A., *Collection mode near-field scanning optical microscopy*, Applied Physics Letters **51**(25), 1987, pp. 2088–2090.

[19] BETZIG E., TRAUTMAN J.K., *Near-field optics: microscopy, spectroscopy, and surface modification beyond the diffraction limit*, Science **257**(5067), 1992, pp. 189–195.

[20] ZEE HWAN KIM, LEONE S.R., *High-resolution apertureless near-field optical imaging using gold nanosphere probes*, The Journal of Physical Chemistry B **110**(40), 2006, pp. 19804–19809.

[21] WEIHUA ZHANG, XUDONG CUI, MARTIN O.J.F., *Local field enhancement of an infinite conical metal tip illuminated by a focused beam*, Journal of Raman Spectroscopy **40**(10), 2009, pp. 1338–1342.

[22] FLEISCHER M., WEBER-BARGIONI A., ALTOE M.V.P., SCHWARTZBERG A.M., SCHUCK P.J., CABRINI S., KERN D.P., *Gold nanocone near-field scanning optical microscopy probes*, ACS Nano **5**(4), 2011, pp. 2570–2579.

[23] DING W., ANDREWS S.R., MAIER S.A., *Internal excitation and superfocusing of surface plasmon polaritons on a silver-coated optical fiber tip*, Physical Review A **75**(6), 2007, article ID 063822.

[24] INOUYE Y., KAWATA S., *Near-field scanning optical microscope with a metallic probe tip*, Optics Letters **19**(3), 1994, pp. 159–161.

[25] BOON-SIANG YEO, WEIHUA ZHANG, VANNIER C., ZENOBI R., *Enhancement of Raman signals with silver-coated tips*, Applied Spectroscopy **60**(10), 2006, pp. 1142–1147.

[26] KALKBRENNER T., RAMSTEIN M., MLYNEK J., SANDOGHDAR V., *A single gold particle as a probe for apertureless scanning near-field optical microscopy*, Journal of Microscopy **202**(1), 2001, pp. 72–76.

[27] ROPERS C., NEACSU C.C., ELSAESSER T., ALBRECHT M., RASCHKE M.B., LIENAU C., *Grating-coupling of surface plasmons onto metallic tips: a nanoconfined light source*, Nano Letters **7**(9), 2007, pp. 2784–2788.

[28] GONCHARENKO A.V., DVOYNENKO M.M., HUNG-CHIH CHANG, JUEN-KAI WANG, *Electric field enhancement by a nanometer-scaled conical metal tip in the context of scattering-type near-field optical microscopy*, Applied Physics Letters **88**(10), 2006, article ID 104101.

[29] GONCHARENKO A.V., HUNG-CHIH CHANG, JUEN-KAI WANG, *Electric near-field enhancing properties of a finite-size metal conical nano-tip*, Ultramicroscopy **107**(2–3), 2007, pp. 151–157.

[30] KANYINDA-MALU C., DE LA CRUZ R.M., *Interface phonon modes in truncated conical self-assembled quantum dots*, Surface Science **529**(3), 2003, pp. 503–514.

[31] CAI Y., MENG Q., EMOTO A., SHIODA T., ONO H., ISHIBASHI T., *FDTD analysis of polarization properties and backscattering coefficients in aperture-less SNOM*, Journal of the Magnetics Society of Japan **38**(3-2), 2014, pp. 127–130.

[32] MARTIN Y.C., HAMANN H.F., WICKRAMASINGHE H.K., *Strength of the electric field in apertureless near-field optical microscopy*, Journal of Applied Physics **89**(10), 2001, pp. 5774–5778.

[33] SUGIURA T., OKADA T., INOUYE Y., NAKAMURA O., KAWATA S., *Gold-bead scanning near-field optical microscope with laser-force position control*, Optics Letters **22**(22), 1997, pp. 1663–1665.

[34] SOBAT Z., SADEGH HASSANI S., *An overview of scanning near-field optical microscopy in characterization of nano-materials*, International Journal of Nano Dimension **5**(3), 2014, pp. 203–212.

[35] BAO W., STAFFARONI M., BOKOR J., SALMERON M.B., YABLONOVITCH E., CABRINI S., WEBER-BARGIONI A., SCHUCK P.J., *Plasmonic near-field probes: a comparison of the campanile geometry with other sharp tips*, Optics Express **21**(7), 2013, pp. 8166–8176.

[36] BOUHELIER A., RENGER J., BEVERSLUIS M.R., NOVOTNY L., *Plasmon-coupled tip-enhanced near-field optical microscopy*, Journal of Microscopy **210**(3), 2003, pp. 220–224.

[37] VACCARO L., AESCHIMANN L., STAUFER U., HERZIG H.P., DÄNDLIKER R., *Propagation of the electromagnetic field in fully coated near-field optical probes*, Applied Physics Letters **83**(3), 2003, pp. 584–586.

[38] ANTOSIEWICZ T.J., WRÓBEL P., SZOPLIK T., *Nanofocusing of radially polarized light with dielectric-metal-dielectric probe*, Optics Express **17**(11), 2009, pp. 9191–9196.

[39] KAZEMI-ZANJANI N., VEDRAINE S., LAGUGNÉ-LABARTHET F., *Localized enhancement of electric field in tip-enhanced Raman spectroscopy using radially and linearly polarized light*, Optics Express **21**(21), 2013, pp. 25271–25276.

[40] HWANG B.S., KWON M.H., JEONGYONG KIM, *Use of a near-field optical probe to locally launch surface plasmon polaritons on plasmonic waveguides: a study by the finite difference time domain method*, Microscopy Research and Technique **64**(5–6), 2004, pp. 453–458.